

PROPERTIES OF MOHR'S FIELD FOR THE STRESS STATE AND THE STRAIN STATE

Anis Sulejmani^{1*}

Mentor Çejku¹

Klodian Dhoska²

Parid Milo¹

Odhisea Koça¹

¹ Mechanical Department, Faculty of Mechanical Engineering, Polytechnic University of Tirana, Albania

² Department of Production & Management, Faculty of Mechanical Engineering, Polytechnic University of Tirana, Albania

ABSTRACT

In the design of different mechanical parts or engineering structures, the stress and strain state of a point or particular points is often required. Finding as many of them as possible will enable us to dimension or select the most optimal possible load or material. Determination of the stress and strain state can be achieved by analyzing this state analytically or graphically with the three circles of Mohr. In this article we will review the grapho-analytical analysis of these Mohr's circles, now considering the space between them as Mohr's space. Thus, in this article are shown the properties of these points of Mohr's field, giving them an analytical and geometrical meaning.

Keywords: Principal stresses or strains, stress or strain tensor, principal orientations, leading cosines, principal Mohr's circles, Mohr space.

1 INTRODUCTION

Different Mohr's Circle is commonly used to represent and analyze stress states in materials, especially in the field of structural and mechanical engineering [1-4]. The Mohr's Circle is a graphical method used in engineering to analyse stress and strain conditions at a point in a material subjected to complex loading [1, 5-10]. The circle is constructed on a set of axes representing normal and shear stresses. The centre of the circle corresponds to the average normal stress, while the radius represents the maximum shear stress [11-17]. Points on the circle represent various stress states associated with different orientations of the planes. Furthermore, it's a valuable tool for gaining insights into stress transformations and is widely employed in fields such as structural design, material testing, and geotechnical engineering [18-28].

Our research work will start by analysing a volumetric element, as shown a tetrahedron in Figure 1. The principal stresses are $\sigma_1, \sigma_2, \sigma_3$ respectively in principal faces.

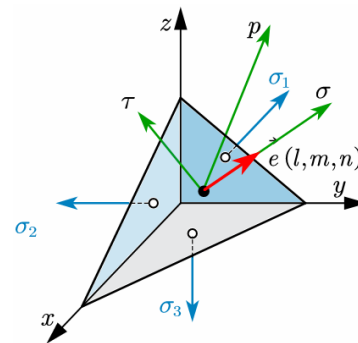


Figure 1 Tetrahedron with principal faces and stresses.

The stress vector on a random face with the leading vector $\vec{e}(l, m, n)$ we will have this matrix form [1] as shown in equation 1:

$$\vec{p} = \begin{pmatrix} p_x \\ p_y \\ p_z \end{pmatrix} = \begin{pmatrix} \sigma_1 & 0 & 0 \\ 0 & \sigma_2 & 0 \\ 0 & 0 & \sigma_3 \end{pmatrix} \begin{pmatrix} l \\ m \\ n \end{pmatrix} = \begin{pmatrix} \sigma_1 l \\ \sigma_2 m \\ \sigma_3 n \end{pmatrix} \quad (1)$$

Whereas, the normal and tangential components of which the normal and tangential stresses are divided respectively would be found by equations 2 and 3. For the normal stress we will have:

$$\sigma = \vec{e} \cdot \vec{p} = (l \ m \ n) \begin{pmatrix} p_x \\ p_y \\ p_z \end{pmatrix} = (l \ m \ n) \begin{pmatrix} \sigma_1 l \\ \sigma_2 m \\ \sigma_3 n \end{pmatrix} \quad (2)$$

While for the shear stress we will have this matrix form, also treated in detail in [1].

Contact author: Anis Sulejmani¹, Mentor Çejku², Klodian Dhoska³, Parid Milo⁴, Odhisea Koça⁵

¹Universiteti Politeknik i Tiranës, Bulevardi Dëshmorët e Kombit Nr. 4, Tiranë
E-mail: asulejmani@fim.edu.al, mcejku@fim.edu.al, kdhoska@fim.edu.al, pmilo@fim.edu.al, okoca@fim.edu.al

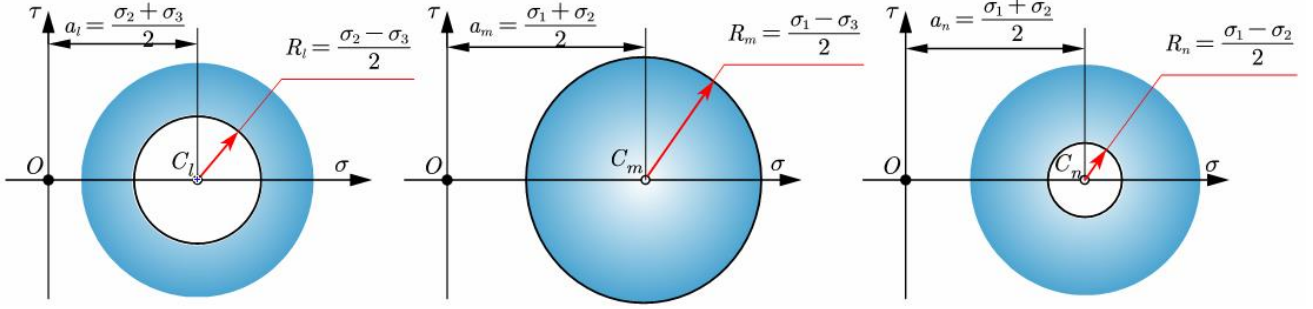


Figure 2 Spaces outside the Mohr's circle for the three leading cosines l , m and n .

$$\vec{\tau} = \vec{p} - \vec{\sigma} = \begin{pmatrix} 1 - l^2 & -lm & -ln \\ -ml & 1 - m^2 & -mn \\ -nl & -nm & 1 - n^2 \end{pmatrix} \begin{pmatrix} p_x \\ p_y \\ p_z \end{pmatrix} \quad (3)$$

From these three matrix forms, after some simplifications, we can explain these in a system of equations as shown below: the equation of driving vector; the normal stress equation as well as total stress equation.

$$1 = l^2 + m^2 + n^2, \text{ the driving vector equation}$$

$$\sigma = \sigma_1 l^2 + \sigma_2 m^2 + \sigma_3 n^2, \text{ the normal stress equation}$$

$$p^2 = \sigma_1^2 l^2 + \sigma_2^2 m^2 + \sigma_3^2 n^2 \text{ total stress equation at a random face.}$$

2 SOLUTIONS OF LEADING COSINES

From the three equations above, let's consider that we have unknown orientations of the random face. So, the task to enter the space of Mohr's field is to determine these orientations first. If we express the above equations in 3x3 matrix form, we would have the expression according to equation 4:

$$\begin{pmatrix} 1 \\ \sigma \\ p^2 \end{pmatrix} = \begin{pmatrix} 1 & 1 & 1 \\ \sigma_1 & \sigma_2 & \sigma_3 \\ \sigma_1^2 & \sigma_2^2 & \sigma_3^2 \end{pmatrix} \begin{pmatrix} l^2 \\ m^2 \\ n^2 \end{pmatrix} \quad (4)$$

This form can be simplified after transformations according to equation 5.

$$\begin{pmatrix} 1 \\ \sigma - \sigma_1 \\ (\sigma - \sigma_1)(\sigma - \sigma_2) + \tau^2 \end{pmatrix} = \begin{pmatrix} 1 & 1 & 1 \\ 0 & \sigma_2 - \sigma_1 & \sigma_3 - \sigma_1 \\ 0 & 0 & (\sigma_3 - \sigma_1)(\sigma_3 - \sigma_2) \end{pmatrix} \begin{pmatrix} l^2 \\ m^2 \\ n^2 \end{pmatrix} \quad (5)$$

It is clear that after this transformation, we can determine step by step the three leading cosines as shown in the solution in vector form in equation 6.

$$\begin{pmatrix} l^2 \\ m^2 \\ n^2 \end{pmatrix} = \begin{pmatrix} \frac{(\sigma - \sigma_2)(\sigma - \sigma_3) + \tau^2}{(\sigma_1 - \sigma_2)(\sigma_1 - \sigma_3)} \\ \frac{(\sigma - \sigma_3)(\sigma - \sigma_1) + \tau^2}{(\sigma_2 - \sigma_3)(\sigma_2 - \sigma_1)} \\ \frac{(\sigma - \sigma_1)(\sigma - \sigma_2) + \tau^2}{(\sigma_3 - \sigma_1)(\sigma_3 - \sigma_2)} \end{pmatrix} \quad (6)$$

3 RESULTS IN THE MOHR'S FIELD

The results of leading cosines l , m and n are mathematically known to be within the segment $-1 \div 1$. Because in equation 6 we have the solution of the square of these cosines, then the segment where this solution should be wanted is $0 \div 1$. Also, using the cyclic rule, we are analyzing only one of these leading cosines, accepting that the solution methodology is the same for all three leading cosines, and in the end we are only giving their analytical and graphical results.

First let's analyze for the leading cosine l and considered unchanged. In equation 7a, b and c, are given the space where the solutions of leading cosines l , m and n are found.

$$0 \leq \left(l^2 = \frac{(\sigma - \sigma_3)(\sigma - \sigma_2) + \tau^2}{(\sigma_1 - \sigma_2)(\sigma_1 - \sigma_3)} \right) \leq 1 \quad (7a)$$

$$0 \leq \left(m^2 = \frac{(\sigma - \sigma_3)(\sigma - \sigma_1) + \tau^2}{(\sigma_2 - \sigma_1)(\sigma_2 - \sigma_3)} \right) \leq 1 \quad (7b)$$

$$0 \leq \left(n^2 = \frac{(\sigma - \sigma_1)(\sigma - \sigma_2) + \tau^2}{(\sigma_3 - \sigma_1)(\sigma_3 - \sigma_2)} \right) \leq 1 \quad (7c)$$

Because from the Strength of Materials we have the agreement $\sigma_1 > \sigma_2 > \sigma_3$ then according to equation 8 we extract the space that is outside the Mohr's circle which achieved when the equation 7a is equal to zero.

$$\left(\sigma - \frac{\sigma_2 + \sigma_3}{2} \right)^2 + \tau^2 \geq \left(\frac{\sigma_2 - \sigma_3}{2} \right)^2 \quad (8)$$

We can do the same analysis for two remaining leading cosines and the result will be a space above or below Mohr's circles. This is because we have to be careful since the solutions are given by equation 6, as well as from the Strength of Materials, we have the agreement for the ranking of the main stresses like $\sigma_1 > \sigma_2 > \sigma_3$.

As for the leading cosine m , the product $(\sigma_2 - \sigma_3)(\sigma_2 - \sigma_1) < 0$, and consequently the space that we take will be restriction from above, that is inside a circle. For the leading cosine n , although both differences are less than zero, the graphed space will be outside the circle. The solution for the other two cases will be given by equations 9 and 10, respectively, for cosines m and n .

$$\left(\sigma - \frac{\sigma_1 + \sigma_3}{2} \right)^2 + \tau^2 \leq \left(\frac{\sigma_1 - \sigma_3}{2} \right)^2 \quad (9)$$

$$\left(\sigma - \frac{\sigma_1 + \sigma_2}{2} \right)^2 + \tau^2 \geq \left(\frac{\sigma_1 - \sigma_2}{2} \right)^2 \quad (10)$$

From figure 2, we clearly see that a stressed state in 3D will be a point which will be located in these Mohr's spaces. We will have special cases when we have a strained plate condition and the points will be located in Mohr's circles. Regarding the cases treated above in equations 7a, b and c, we considered that this leading cosine is greater than zero. But what happens in other cases, because we look for it in the segment. $0 \div 1$?

4 GRAPH OF MOHR'S CIRCLES IN HIS SPACE

To graphically show Mohr's circles in the area defined in figure 2 we will have to analyse the case where these leading cosines are constant. In the equation 6 let consider that the leading cosine l is constant and determined by $l = \cos \alpha$. After some transformation, we can get $(\sigma - \sigma_3)(\sigma - \sigma_2) + \tau^2 = (\sigma_1 - \sigma_2)(\sigma_1 - \sigma_3)l^2$. Then with the same transformations we determine equation 11, where we have:

$$(\sigma - a_l)^2 + \tau^2 = \left(\frac{\sigma_2 - \sigma_3}{2}\right)^2 + (\sigma_1 - \sigma_2)(\sigma_1 - \sigma_3)l^2 \quad (11)$$

Where $a_l = \frac{\sigma_2 + \sigma_3}{2}$, is the center of concentric circles with radius according to the equation 12.

$$R_l(l) = \sqrt{\left(\frac{\sigma_2 - \sigma_3}{2}\right)^2 + (\sigma_1 - \sigma_2)(\sigma_1 - \sigma_3)l^2} \quad (12)$$

It seems clear that this equation depends on the leading cosine and this geometrically expresses concentric circles passing from the center of a_l . Special cases when $l = 0$ and $l = 1$, which present the point in the circle and the rays respectively will be: $R_{l=0} = \frac{\sigma_2 - \sigma_3}{2}$ and $R_{l=1} = \sigma_1 - \frac{\sigma_2 + \sigma_3}{2}$. With the same reasoning for the other two leading cosines, the solution of the rays of the concentric circles respectively in their centers $a_m = \frac{\sigma_1 + \sigma_3}{2}$ and $a_n = \frac{\sigma_1 + \sigma_2}{2}$ will be according to equations 13 and 14.

$$R_m(m) = \sqrt{\left(\frac{\sigma_1 - \sigma_3}{2}\right)^2 + (\sigma_2 - \sigma_1)(\sigma_2 - \sigma_3)m^2} \quad (13)$$

$$R_n(n) = \sqrt{\left(\frac{\sigma_1 - \sigma_2}{2}\right)^2 + (\sigma_3 - \sigma_1)(\sigma_3 - \sigma_2)n^2} \quad (14)$$

Special cases will be for cosines m and n respectively $R_{m=0} = \frac{\sigma_1 - \sigma_3}{2}$ and $R_{m=1} = \sigma_2 - \frac{\sigma_1 + \sigma_3}{2}$, as well $R_{n=0} = \frac{\sigma_1 - \sigma_2}{2}$ and $R_{n=1} = \frac{\sigma_1 + \sigma_2}{2} - \sigma_3$.

Equations 12, 13 and 14 express the equations of the rays of concentric circles according their centers. Let's express it graphically in a case where we know the stress tensor as follows:

$$T_\sigma = \begin{pmatrix} \sigma_{xx} & \sigma_{xy} & \sigma_{xz} \\ \sigma_{yx} & \sigma_{yy} & \sigma_{yz} \\ \sigma_{zx} & \sigma_{zy} & \sigma_{zz} \end{pmatrix} = \begin{pmatrix} 4.25 & 0.65 & 1.125 \\ 0.65 & -1.562 & 2.49 \\ 1.125 & 2.49 & 1.312 \end{pmatrix} \quad (15)$$

The principal stresses for this stress tensor will be $\sigma_1 = 5, \sigma_2 = 2, \sigma_3 = -3$. Then, we can make the dependence of

Mohr's circles in function of the respective leading angles. Figure 3 shows the relationships of these rays for the given tensor as a function of the leading cosines in the same graph.

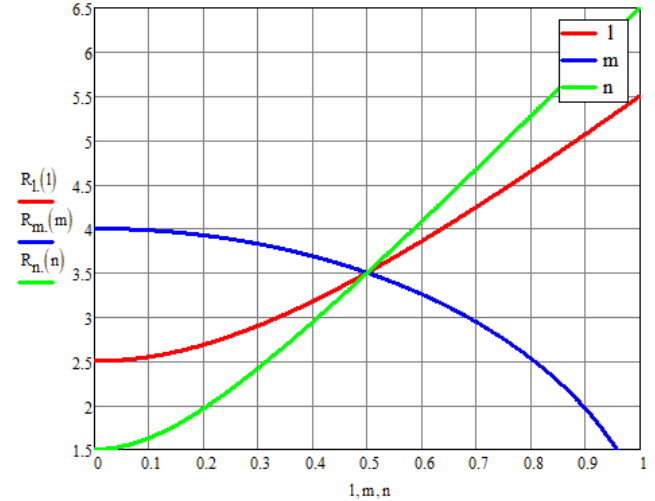


Figure 3 The dependence of the rays of circles with the corresponding leading cosines.

From the graph of figure 3, for a different stress state, we can conclude that the rays of the main circles in Mohr's space are equal if the leading cosines are $l = m = n = 0.5$. We must be careful since this point has 3 faces in Mohr's space, although the rays are equal for all 3 leading cosines, the centers of these circles are different. This expression can also be derived from equations 12, 13 and 14. If we replace these leading cosines, we will have equation 24.

$$R_l(l)^2 = \left(\frac{\sigma_2 - \sigma_3}{2}\right)^2 + (\sigma_1 - \sigma_2)(\sigma_1 - \sigma_3)l^2 \quad (16)$$

For $l = 0.5$

$$R_l(0.5)^2 = \left(\frac{\sigma_2 - \sigma_3}{2}\right)^2 + (\sigma_1 - \sigma_2)(\sigma_1 - \sigma_3)\frac{1}{4} \quad (17)$$

$$R_l(0.5)^2 = \frac{1}{4}(\sigma_1^2 + \sigma_2^2 + \sigma_3^2 - \sigma_1\sigma_2 - \sigma_2\sigma_3 - \sigma_1\sigma_3) \quad (18)$$

$$(\sigma_1 + \sigma_2 + \sigma_3)^2 = \sigma_1^2 + \sigma_2^2 + \sigma_3^2 + 2(\sigma_1\sigma_2 + \sigma_2\sigma_3 + \sigma_1\sigma_3) \quad (19)$$

$$\sigma_1^2 + \sigma_2^2 + \sigma_3^2 = (\sigma_1 + \sigma_2 + \sigma_3)^2 - 2(\sigma_1\sigma_2 + \sigma_2\sigma_3 + \sigma_1\sigma_3) \quad (20)$$

$$R_l(0.5)^2 = \frac{1}{4}[(\sigma_1 + \sigma_2 + \sigma_3)^2 - 3(\sigma_1\sigma_2 + \sigma_2\sigma_3 + \sigma_1\sigma_3)] \quad (21)$$

$$I_1 = \sigma_1 + \sigma_2 + \sigma_3 \quad (22)$$

$$I_2 = \sigma_1\sigma_2 + \sigma_2\sigma_3 + \sigma_1\sigma_3 \quad (23)$$

$$R_l(0.5)^2 = \frac{1}{4}(I_1^2 - 3I_2) = I_4 \quad (24)$$

Will have the same expressions for $m = 0.5$ or $n = 0.5$.

So, the term $\sigma_1^2 + \sigma_2^2 + \sigma_3^2 - \sigma_2\sigma_3 - \sigma_2\sigma_3 - \sigma_2\sigma_3$ is the same for all three leading cosines.

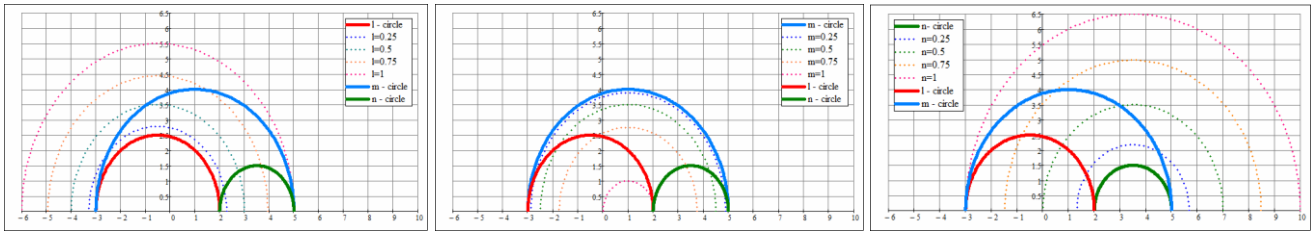


Figure 4 Mohr's l , m and n concentric circles in his space.

If we express equation 11 and the analogous equations for the cosine m and n as their function, than we would obtain graphically the concentric circles for this example, figure 4. Since they are the two extreme cases for the leading cosine equal to zero and equal to one, we have the two restrictions of these circles. Circles whose rays increase, circles l and n are bounded from below by the zero circle (the special case of Mohr, as in plane stress state) and from above when it interrupts the other main stress. While in the case of decreasing circles, it is either restrictions from above by the largest Mohr circle and from below when this circle becomes tangent to the other two at the same point σ_2 . All the concentric circles of Mohr shown in figure 4 must be restricted by the other two circles of leading. This will be given with the conditions of the minimum and maximum angles of the making of these circles. For this, let's look at a circle with constant l .

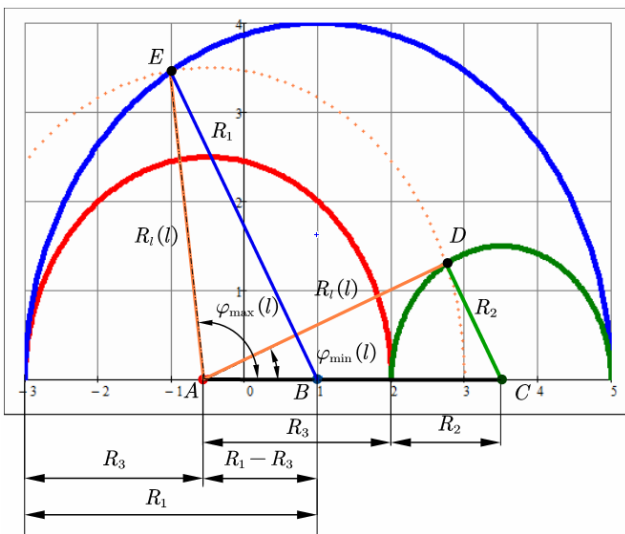


Figure 5 Minimum and maximum angles of particular points in Mohr's space for l .

Analysing the two triangles, ACD and ABE at figure 5, we have the expressions for the minimum and maximum angles as in equations 25 and 26.

$$\varphi_{min}(l) = \cos^{-1} \left(\frac{R_l(l)^2 + (R_2 + R_3)^2 - R_2^2}{2 \cdot R_l(l) \cdot (R_2 + R_3)} \right) \quad (25)$$

$$\varphi_{max}(l) = \cos^{-1} \left(\frac{R_l(l)^2 + (R_1 - R_3)^2 - R_1^2}{2 \cdot R_l(l) \cdot (R_1 - R_3)} \right) \quad (26)$$

Graphically, these two angles would be given as in figure 6. We can follow the same rationalization for the two other circles. Regarding the geometry for determining the minimum angles for the case of the cosine m , we analyze the triangles BCF and BAG in figure 7.

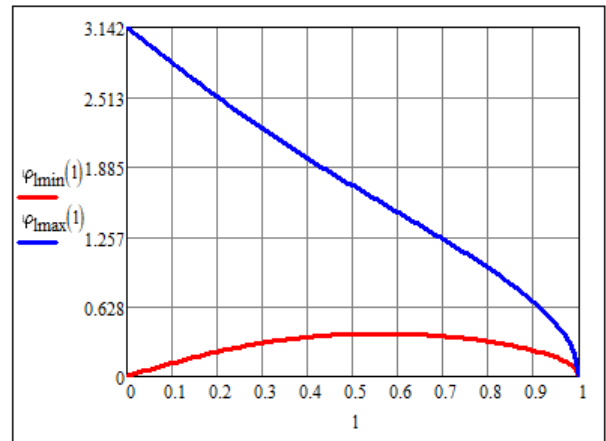


Figure 6 Graphs of the minimum and maximum angle of the leading cosine l .

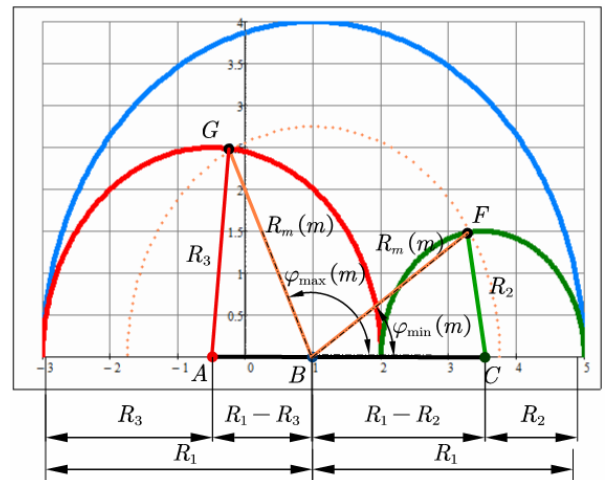


Figure 7 Minimum and maximum angles of particular points in Mohr's space for m .

The minimum and maximum angles in function of the leading cosine m will be respectively according to equations 27 and 28.

$$\varphi_{min}(m) = \cos^{-1} \left(\frac{R_m(m)^2 + (R_1 - R_2)^2 - R_2^2}{2 \cdot R_m(m) \cdot (R_1 - R_2)} \right) \quad (27)$$

$$\varphi_{max}(m) = \pi - \cos^{-1} \left(\frac{R_m(m)^2 + (R_1 - R_3)^2 - R_3^2}{2 \cdot R_m(m) \cdot (R_1 - R_3)} \right) \quad (28)$$

Graphically, these angles would be given according to figure 8. Also for the third case we analyze figure 9, and respectively the triangles CBM and CAN.

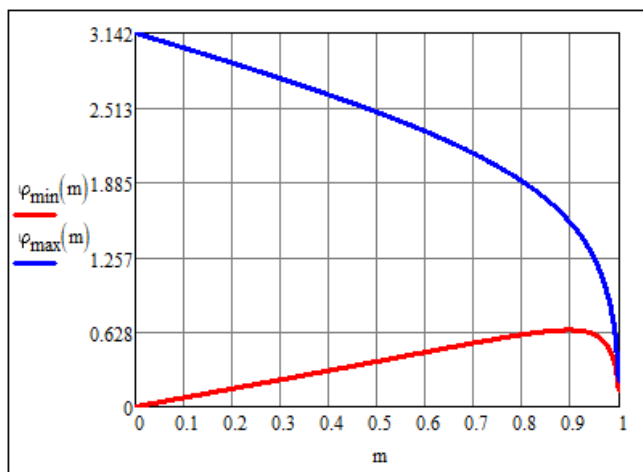


Figure 8 Graphs of the minimum and maximum angle of the leading cosine m .

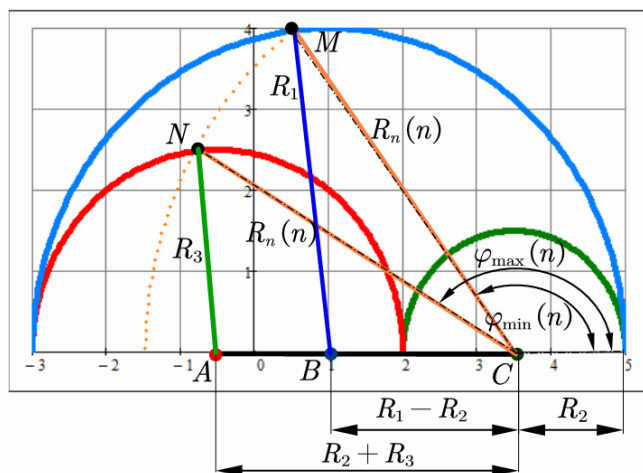


Figure 9 Minimum and maximum angles of particular points in Mohr's space for n .

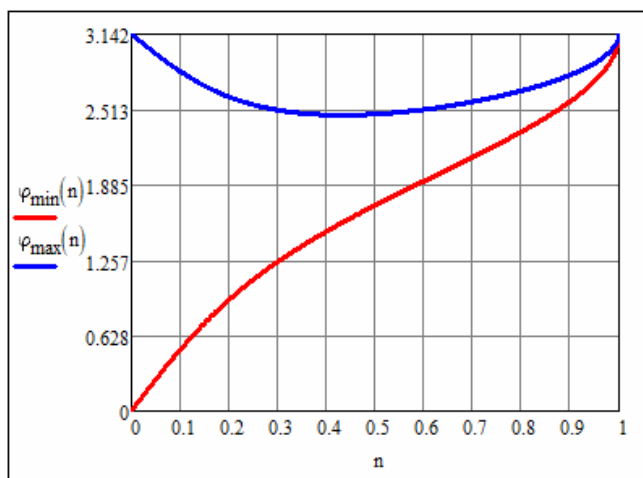


Figure 10 Graphs of the minimum and maximum angle of the leading cosine n .

The minimum and maximum angles as a function of the leading cosine n will be respectively according to equations 29 and 30.

$$\varphi_{min}(n) = \pi - \cos^{-1}\left(\frac{R_n(n)^2 + (R_1 - R_2)^2 - R_1^2}{2 \cdot R_n(n) \cdot (R_1 - R_2)}\right) \quad (29)$$

$$\varphi_{max}(n) = \pi - \cos^{-1}\left(\frac{R_n(n)^2 + (R_2 + R_3)^2 - R_3^2}{2 \cdot R_n(n) \cdot (R_2 + R_3)}\right) \quad (30)$$

Graphically, according to the leading cosine n , these angles will give in to figure 10.

Taking equations of maximum and minimum angles, which in Mohr's space express the minimum and maximum borders which a different face it can rotate around the direction of the main stresses, then we can make Mohr's grid. Let's make these rotations in the example taken as in figure 1. As seen in this figure, is formed Mohr's grid which for a different face it shows the path of rotation until it gets to the Mohr's face.

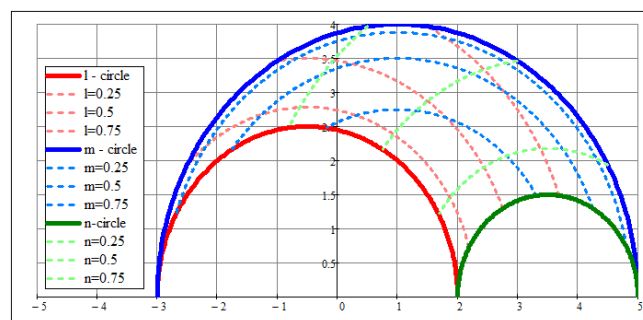


Figure 11 Graphs of the grid in Mohr's space. Let's also analyses the cases where $l = m = n = 0.5$, as a single point in circles's graph (figure 3), but this give three points in Mohr's space which represented by points A, B and C. Analysing the triangles for minimum and maximum angles, the angles will be in function of three leading cosines. So the maximum and minimum rotations for each leading cosine will be given by the equations as follows:

$$\varphi_l(l, m, n) = \cos^{-1}\left(\frac{R_l(l)^2 + (R_2 + R_3)^2 - R_n(n)^2}{2 \cdot R_l(l) \cdot (R_2 + R_3)}\right) \quad (31)$$

$$\varphi_m(l, m, n) = \cos^{-1}\left(\frac{R_m(m)^2 + (R_1 - R_2)^2 - R_n(n)^2}{2 \cdot R_m(m) \cdot (R_1 - R_2)}\right) \quad (32)$$

$$\varphi_n(l, m, n) = \pi - \cos^{-1}\left(\frac{R_n(n)^2 + (R_1 - R_2)^2 - R_m(m)^2}{2 \cdot R_n(n) \cdot (R_1 - R_2)}\right) \quad (33)$$

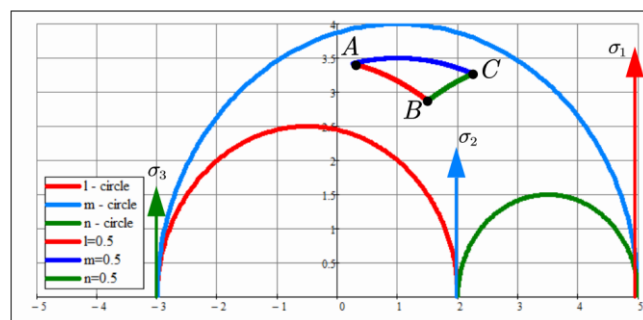


Figure 12 Mohr's space analysis.

5 CONCLUSIONS

In our study work, the Mohr cycle has significantly contributed to the advancement of engineering practices related to fatigue analysis, material characterization, and structural design, leading to the development of safer and more durable mechanical systems. Here are some specific achievements associated with the Mohr cycle study:

- Plotting stress and strain values for each cycle, engineers can identify fatigue failure points and determine the number of cycles a material can withstand before failure.
- Understanding the stress and strain distribution through the Mohr cycle helps in identifying potential failure modes and taking preventive measures. This could involve implementing design modifications, introducing stress-relieving features, or applying surface treatments to improve material durability.
- When the leading cosines are $l = m = n = 0.5$, their respective rays are equal.
- The expression for these rays is $\frac{1}{4}(\sigma_1^2 + \sigma_2^2 + \sigma_3^2 - \sigma_2\sigma_3 - \sigma_2\sigma_3 - \sigma_2\sigma_3)$.
- A simplified form of this above expression is given according equation 24. This equation is fourth invariant which give the rays in as stress state where the leading cosines are two by two equal to 0.5.
- Mohr's main circles represent orientations with zero leading cosines.
- Mohr's grid circles are concentric circles centered on the main Mohr's circles.
- They are restricted by the main Mohr's circles and the extremal angles are given by expressions 31, 32 and 33.

REFERENCES

- [1] Sulejmani, A., Koça, O., Cejku, M. Graphical and Analytical Analysis in the Field of Mohr's Circles. *Lecture Notes on Multidisciplinary Industrial Engineering*. Springer, Cham. Part F2090, pp. 166–181, 2024.
- [2] Sulejmani, A., Koça, O., Dhoska, K. Method of principal orientation in Mohr's space. *J. Southwest Jiaotong Univ.*, Vol. 58 No. 2, pp. 178-187, 2023.
- [3] Zhang, T., Lin, S., Zheng, H., Chen, Y.: Elastoplastic integration method of mohr-coulomb criterion. *Geotechnics*, Vol. 2 No. 3, pp. 599-614, 2022.
- [4] Martin, C.M., Makrodimitropoulos, A. Finite-element limit analysis of Mohr-Coulomb materials in 3D using semidefinite programming. *J. Eng. Mech.*, Vol. 134 No. 4, pp. 339-347, 2008.
- [5] Xu, S.S., Nieto-Samaniego, A.F., Alaniz-Álvarez, S.A. 3D Mohr diagram to explain reactivation of pre-existing planes due to changes in applied stresses. In: *ISRM International Symposium on In-Situ Rock Stress*, pp. ISRM–ISRS. 2010.
- [6] Sulejmani, A., & Koça, O. Development of Optimal Transmission Rate of the Kinematic Chain by using Genetic Algorithms Coded in Mathcad. *International Journal of Innovative Technology and Interdisciplinary Sciences*, Vol. 4 No. 4, pp. 792-803. 2021.
- [7] Lumi, D., Sulejmani, A., Dhoska, K., Koça, O. Study of the strengthened state near the forces for the semi-plan. *Pollack Periodica*, Vol. 17 No. 2, pp. 98–103, 2022.
- [8] Sulejmani, A., Koça, O., Dhoska, K., Gheibi, M., Moezzi, R.: A novel method of jacobian contours to evaluate the influence line in statically determinate structures. *Applied Mechanics*, Vol. 4 No. 4, pp. 1172–1187, 2023.
- [9] Housner, G.W., and Hudson, D.E. *Applied Mechanics: Dynamics*, U.S., 1991.
- [10] Li, Y., Yang, Y., Yu, H.S., and Roberts, G. Principal stress rotation under bidirectional simple shear loadings. *KSCE Journal of Civil Engineering*, Vol. 22 No. 5, pp. 1651-1660, 2018.
- [11] Koça, O., Sulejmani, A., Alimhilli, P., Direct method of rigidity using Mathcad software. *IOP Conference Series: Materials Science and Engineering*, Vol. 1024 No. 1, p. 012093, 2021.
- [12] Dhoska, K., Tola, S., Pramono, A., and Vozga, I. Evaluation of measurement uncertainty for the determination of the mechanical resistance of the brick samples by using uniaxial compressive strength test. *International Journal of Metrology and Quality Engineering*, Vol. 9 No. 12, pp. 1-5, 2018.
- [13] Bidaj, A., Hysenlliu, M. Reinforcement Application Techniques in Earthquake Damaged Buildings Caused at Central Part of Albania. *Journal of Integrated Engineering and Applied Sciences*, Vol. 1 No. 1, pp. 14-22, 2023.
- [14] Dhoska, K., Lumi, D., Sulejmani, A., Koça, O. Measurement uncertainty for mechanical resistance of manufactured steel bar. *Pollack Periodica*, Vol. 17 No. 2, pp. 104–108, 2022.
- [15] Hysenlliu, M., & Deneko, E. Capacity Evaluation and Spectral Analysis of Damaged Low-Rise Reinforced Concrete Building. *Journal of Transactions in Systems Engineering*, Vol. 1 No. 3, pp. 120-130, 2023.
- [16] Pramono, A., Nugraha, K., Suryana, Milandia, A., & Juniarsih, A. Design of Rolling Machine to Improve Mechanical Properties of Strapping-band Steel and Low Carbon Steel type SHP 440. *International Journal of Innovative Technology and Interdisciplinary Sciences*, Vol. 5 No. 1, pp. 822-832, 2022.
- [17] Dhoska K., Markja I., Bebi E., Sulejmani A., Koça O., Sita E., Pramono A. Manufacturing Process of the Aluminum Alloy AA6063 for Engineering Applications, *Journal of Integrated Engineering and Applied Sciences*. Vol. 1 No. 1, 1-13, 2023.

- [18] Sulejmani, A., Koça, O., Milo, P. Analyzation of General Displacements of Mechanical Structures Using Self-equilibrated Forces. *Lecture Notes on Multidisciplinary Industrial Engineering*. Springer, Cham. Part F2090, pp. 182–193, 2024.
- [19] Peacock, D.C.P., Sanderson, D.J., and Leiss, B. Use of Mohr's diagrams to predict fracturing in a potential geothermal reservoir. *Geosciences*, Vol. 11, pp. 1-27, 2021.
- [20] Wani, B.S. Analytical study on the influence of rib beams on the stability of RCC dome structures. *International Journal of Innovative Technology and Interdisciplinary Sciences*, Vol. 3 No. 3, pp. 480-489, 2020.
- [21] Koça, O., Sulejmani, A., Dhoska, K. Pressure distribution on rolling-slide contact problem. *Pollack Periodica*, Vol. 16, No. 1, pp. 71-76, 2021.
- [22] Pramono, A., Dhoska, K., Markja, I., Kommel, L. Impact pressure on mechanical properties of aluminum based composite by ECAP-parallel channel. *Pollack Periodica*, Vol. 14 No. 1, pp. 67-74, 2019.
- [23] Gufler, V., Wehrle, E., Vidoni R. Analytical sensitivity analysis of flexible multibody dynamics with index-1 differential-algebraic equations and Baumgarter stabilization. *International Journal of Mechanics and Control*, Vol. 24, No. 1, pp. 3-14, 2023.
- [24] Koka, K., Dhoska, K., & Bylykbashi A. Analysis of Vibration and Acoustic Sound Radiation of a Rotationally Symmetrical Plate. *Journal of Transactions in Systems Engineering*, Vol. 2, No. 1, pp. 156-169, 2024.
- [25] P. Akpan, P., Biamene B, N., Ifionu S., E., Gloria, D.-O. I., J. Gospel, K., & D. Burabe, A.-B. Validation of the Hydrostatic Position of a Partially and Fully Submerged Vertical Curved Plane Surface Apparatus. *International Journal of Innovative Technology and Interdisciplinary Sciences*, Vol. 6, No. 3, pp. 1206–1219, 2023.
- [26] Goti, E., & Curà F.M. Friction torque in thrust ball bearings lubricated by graphene-enriched grease with a modified pin-on-disc method. *International Journal of Mechanics and Control*, Vol. 24, No. 1, pp. 207-214, 2023.
- [27] Korytov, M.S., Shcherbakov, V.S., Kashapova I.E., Investigation of dynamic characteristics of the vibration isolation system for operators' seats. *International Journal of Mechanics and Control*, Vol. 24, No. 2, pp. 19-26, 2023.
- [28] Mishra, J., & Panigrahi, R. Mini-Review on Structural Performance of Fiber Reinforced Geopolymer Concrete. *International Journal of Innovative Technology and Interdisciplinary Sciences*, Vol. 3, No. 2, pp. 435–442. 2020.

